COMMUNICATIONS PHYSICS

ARTICLE

DOI: 10.1038/s42005-018-0052-1 OPEN

Spin-wave interference in magnetic vortex stacks

Carolin Behncke [1], Christian F. Adolff[1], Nicolas Lenzing[2], Max Hänze[3], Benedikt Schulte[4], Markus Weigand[5], Gisela Schütz[5] & Guido Meier[4]

Spin waves with wavelengths in the nanometre range could serve as data carriers in future magnonic logic or signal processing devices. We investigate the interference of spin waves emitted from magnetic vortices in two exchange-coupled vortex stacks. The spin-wave dynamics are studied using scanning transmission X-ray microscopy and micromagnetic simulations. Stacks of vortices provide an excellent controllability of spin-wave properties including a tunable wavelength in the 100 nm regime and manipulation of their propagation direction via the magnetisation configuration. Furthermore, interference gives rise to amplified or reduced spin-wave amplitudes in distinct areas of the structure providing controlled confinement crucial for future applications of spin waves.

[1] The Hamburg Centre for Ultrafast Imaging, Luruper Chaussee 149, 22761 Hamburg, Germany. [2] Institut für Angewandte Physik und Zentrum für Mikrostrukturforschung, Universität Hamburg, Jungiusstr. 11, 20355 Hamburg, Germany. [3] Max-Planck Institute for Solid State Research, Heisenbergstr. 1, 70569 Stuttgart, Germany. [4] Max-Planck Institute for the Structure and Dynamics of Matter, Luruper Chaussee 149, 22761 Hamburg, Germany. [5] Max-Planck Institute for Intelligent Systems, Heisenbergstr. 3, 70569 Stuttgart, Germany. Correspondence and requests for materials should be addressed to C.B. (email: cbehncke@physnet.uni-hamburg.de)

Spin waves are promising candidates as a building block for future magnonic logic or signal processing devices[1–5]. Having full control over the spin waves is fundamental for the realisation of such devices. Interference phenomena can be used to spatially confine the information that is essential for the application of spin waves[6–9]. Recently it has been shown that stacked vortex structures are efficient emitters of spin waves with tunable wavelength[10]. Spin waves emitted from these vortex stacks have a wavelength in the order of magnitude of 100 nm and thus open a path to miniaturisation.

The magnetic vortex is the ground-state magnetisation configuration in ferromagnetic nanodisks of fitting geometry[11]. The magnetisation circulates in the plane around the vortex core in the centre region, where the magnetisation points out-of-plane. The orientation of the magnetisation in the vortex core is characterised by the polarisation ($p = \pm 1$)[12], where a positive polarisation signifies an upwards-pointing magnetisation. The circularity describes the sense of the in-plane curling ($c = \pm 1$), where a positive circularity represents a counter-clockwise rotation of the magnetisation. When excited by magnetic fields or electric currents, the vortex core gyrates around its centre position[13,14]. The resonance frequency of this gyrotropic mode lies in the sub-gigahertz regime[15,16]. The sense of gyration depends on the polarisation of the core[13]. Besides the gyrotropic mode, the vortex can be excited to higher-order spin-wave modes[17–19]. When excited with frequencies in the gigahertz regime, the vortex performs a low-amplitude gyration. A stack of two vortices can then serve as spin-wave emitter with a linear dispersion relation and thus tunable wavelength[10].

We report a direct observation of interferences of spin waves in two exchange-coupled vortex stacks (see Fig. 1a). We use micromagnetic simulations[20] and scanning transmission X-ray microscopy (STXM) measurements at the MAXYMUS microscope of the BESSY II synchrotron in Berlin, Germany, to observe the spin-wave dynamics temporally and spatially resolved. Different stable magnetisation configurations and their dynamic response to high-frequency magnetic fields are investigated. The transient behaviour of one particularly interesting magnetisation state is discussed in more detail. Spin waves emitted by the vortex stacks interfere with each other, resulting in different interference patterns dependent on their magnetisation state. The interference leads to an amplification or reduction of travelling spin waves in distinct points in space. In the experiments, we directly observe spin-wave interference and also spin-wave diffraction patterns.

Results

Samples and magnetisation configurations. The investigated structures are two coupled stacks of disks with a radius $r = 800$ nm and an overlap $o = 300$ nm (Fig. 1b). The stacks consist of two permalloy layers with a thickness $t_{\mathrm{Py}} = 50$ nm that are separated and covered by silicon layers of $t_{\mathrm{Si}} = 10$ nm (Fig. 1c). For the excitation of spin waves, the structures are placed upon a coplanar waveguide. A high-frequency current sent through the waveguide leads to a unidirectional high-frequency magnetic field H_{rf} that excites the magnetisation dynamics (see Fig. 1a). In the simulations, the structures are slightly smaller ($r = 640$ nm) but have the same aspect ratio $\frac{t_{\mathrm{Py}}}{r}$ and percentile overlap so that they have equal resonance frequencies[15]. Here, the 10 nm spacing between the layers is modelled using vacuum. Due to the overlap, the disks in one layer are exchange coupled. The spacing between the layers prevents an exchange coupling in z-direction and the interlayer coupling is dipolar.

Each layer of the stack contains two vortices, leading to an overall number of four vortices in the structure. Each disk can have a polarisation $p = \pm 1$ and a circularity $c = \pm 1$. There are

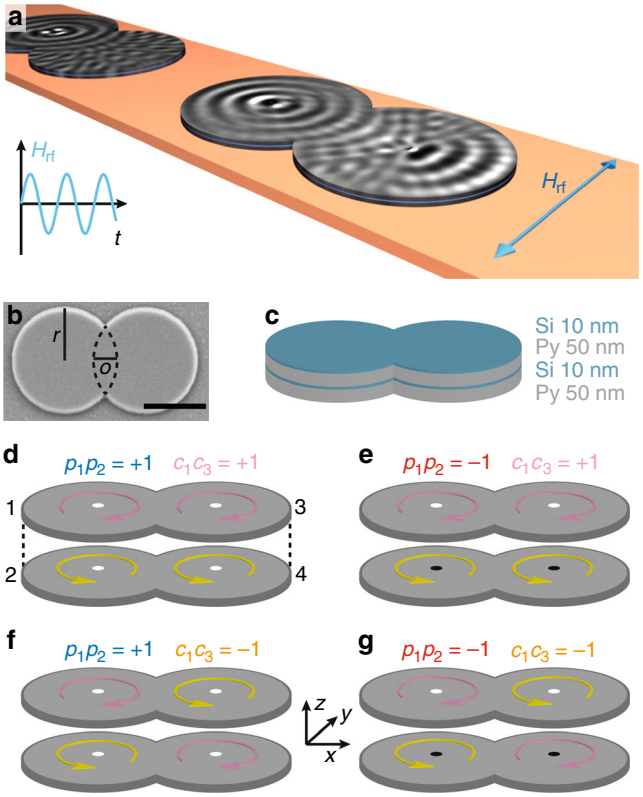

Fig. 1 Two exchange-coupled stacks of magnetic vortices. **a** Schematic representation of the investigated vortex system. The black and white contrast on the structures corresponds to exemplary micromagnetic simulations of the spin-wave dynamics. The structures are placed on a coplanar waveguide. The inset shows the high-frequency field used to excite the vortex dynamics. **b** Scanning electron micrograph of the investigated sample (1 μm scale bar). **c** Schematic representation of the structures consisting of two permalloy layers separated and covered by silicon layers. **d**–**g** Exemplary configurations of the polarisations p_i and the circularities c_i of the vortices (1–4, indicated in **d**). The yellow and pink arrows correspond to a circularity of $c = +1$ and $c = -1$, respectively. The white and black dots represent a polarisation of $p = +1$ and $p = -1$, respectively

thus four possible (c, p)-configurations per disk and $4^4 = 256$ possible (c, p)-configurations of the whole structure. We will concentrate on highly symmetric states with differing circularities for the upper and lower disks, i.e. $c_1c_2 = -1$ and $c_3c_4 = -1$. Only for such circularity configurations there exist spin-wave modes with short wavelengths in the 100 nm regime[10]. Four highly symmetric (c, p)-configurations are schematically depicted in Fig. 1d–g. The white and black dots represent a positive and negative polarisation and the yellow and pink arrows indicate a positive and negative circularity, respectively. We distinguish between states with all positive polarisations (blue: $p_1p_2 = +1$ and $p_3p_4 = +1$, Fig. 1d, f) and with opposite polarisations in the upper and lower disks (red: $p_1p_2 = -1$ and $p_3p_4 = -1$, Fig. 1e, g). For these polarisation configurations, states with equal circularities in a layer (pink: $c_1c_3 = +1$ and $c_2c_4 = +1$, Fig. 1d, e) and opposite circularities (orange: $c_1c_3 = -1$ and $c_2c_4 = -1$, Fig. 1f, g) are considered. Based on symmetry considerations it is sufficient to indicate the polarisations in one stack (p_1p_2) and the circularities in one layer (c_1c_3).

Micromagnetic simulations of magnetisation configurations. Micromagnetic simulations are performed to investigate the four

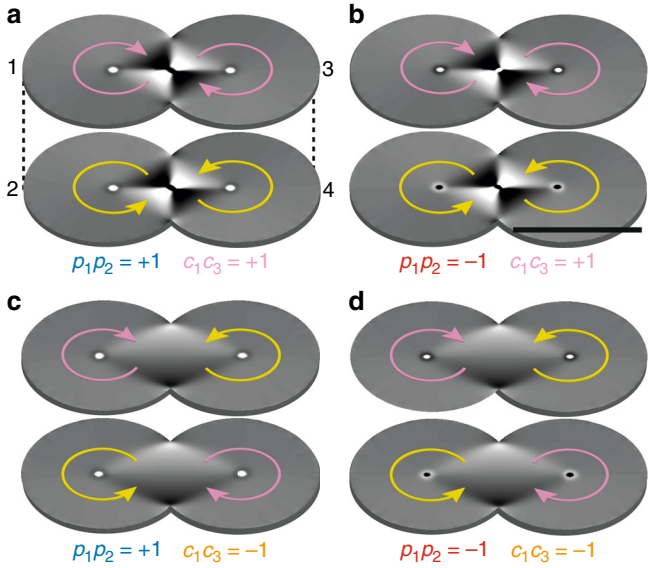

Fig. 2 Micromagnetic simulations of stable magnetisation configurations. The two layers are shown in a perspective view. The black and white contrast shows the z-component of the magnetisation M_z summed up for each layer individually. It is oversaturated for better visibility. The yellow and pink arrows represent the in-plane magnetisation, i.e. a circularity of $c = +1$ and $c = -1$, respectively. **a**, **b** show an antivortex state with equal circularities in the plane. In **a** all polarisations are equal, in **b** the polarisations of the vortices on top of each other differ. **c**, **d** exhibit a diamond magnetisation state where the circularities in the plane differ. In **c** all polarisations are equal, in **d** the polarisations in the stacks differ. Scale bar: 1 μm

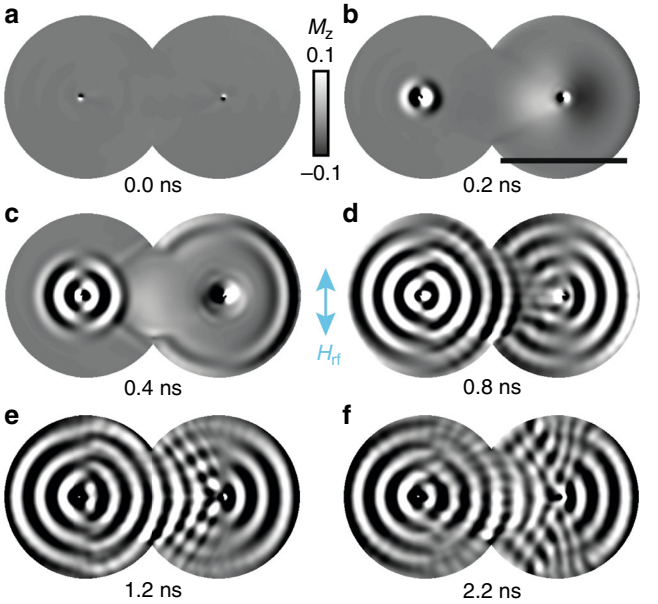

Fig. 3 Transient behaviour of the spin-wave interference. Micromagnetic simulations of the sum of the z-component of the magnetisation M_z over both layers of a diamond state with different polarisations in the stacks (see Fig. 2d). For better visibility the static contrast is subtracted and the contrast is oversaturated. The colour scale indicates the visible range of M_z in terms of the saturation magnetisation. **a**–**f** show snapshots after switching on a high-frequency magnetic field $\mu_0 H_{rf} = 0.5$ mT with a frequency of $f_{rf} = 6$ GHz after **a** 0 ns, **b** 0.2 ns, **c** 0.4 ns, **d** 0.8 ns, **e** 1.2 ns, and **f** 2.2 ns. Scale bar: 1 μm

selected magnetisation configurations. Figure 2 shows these magnetisation states with the (c, p)-configurations suggested in Fig. 1d–g. The black and white contrast corresponds to the z-component of the magnetisation M_z summed up for each layer individually. The pink and yellow arrows indicate the M_x and M_y components. Magnetisation states with equal circularities in each layer ($c_1c_3 = +1$) are depicted in Fig. 2a, b. Besides the vortices in each disk, these magnetisation states feature a stack of two antivortices[21] in the centre of the structure. Magnetic moments pointing in opposite in-plane directions in the overlap region are energetically unfavourable. Therefore, antivortices are formed in the centre region. This magnetisation state is predicted for equal polarisations ($p_1p_2 = +1$, Fig. 2a) and opposite polarisations ($p_1p_2 = -1$, Fig. 2b) in the stacks. The antivortices in the stack have the same relative polarisations as the vortices. In Fig. 2a both the antivortices have a negative (black) polarisation, while in Fig. 2b the polarisations of the antivortices differ.

Apart from the antivortex state, a magnetisation state is formed that shows different circularities of the disks of the same layer (Fig. 2c, d). This state is referred to as diamond state. Here, the magnetic moments in the overlap region point in the same direction. This magnetisation state is observed for equal (Fig. 2c) and opposite (Fig. 2d) polarisations in the stacks. All of the highly symmetric (c, p)-configurations considered in Fig. 1d–g are thus confirmed by micromagnetic simulations to be possible stable magnetisation states. Depending on the c-configurations, antivortex and diamond magnetisation states emerge. These simulated stable magnetisation configurations are indeed observed experimentally (see Supplementary Note 1, Supplementary Fig. 1 for magnetic force micrographs of the magnetisation states).

Micromagnetic simulations of spin-wave dynamics. We investigate the formation of spin waves in exchange-coupled vortex stacks, first taking the example of a diamond magnetisation state with differing polarisations in the stacks (Fig. 2d). The transient magnetisation dynamics are depicted as snapshots in Fig. 3 at different times after switching on a high-frequency magnetic field in y-direction. The excitation frequency is $f_{rf} = 6$ GHz and the magnetic field amplitude is $\mu_0 H_{rf} = 0.5$ mT. In the Supplementary Material the corresponding movie (Supplementary Movie 1) is available. In the beginning, the vortices rest and only the black and white contrast of the vortex cores in the centre of the disks is visible (Fig. 3a). After 0.2 ns (Fig. 3b) the emission of spin waves with a wavelength of 170 nm by the left vortex cores is observed. The right cores emit spin waves with a far longer wavelength of approximately 900 nm. In Fig. 3c an inwards-travelling mode with a short wavelength of 170 nm emerges at the edges of the right stack. This is a result of a non-reciprocal reflection of the long-wavelength mode that is emitted by the right vortices. The short-wavelength mode emitted by the left vortices travels to the right stack (Fig. 3d) and interferes with the reflected mode (Fig. 3e, f). A further investigation of this simulation data (see also Supplementary Movie 2) reveals that both stacks emit a long and a short-wavelength mode as observed in ref.[10]. These two modes propagate in opposite directions, depending on the absolute circularity configuration in a stack. The propagation directions of the long and the short spin-wave modes are thus topologically protected.

In the following, the spin-wave interferences are studied for all stable magnetisation configurations introduced in Fig. 2. In Fig. 4a–d snapshots of the steady state spin-wave emission are depicted (see also Supplementary Movie 3). In Fig. 4a the dynamic response of an antivortex state with equal polarisations is depicted. Spiral-shaped, propagating spin waves with a wavelength of 90 nm are emitted by the vortex cores. The spin waves travel outwards as indicated by the white arrows. The

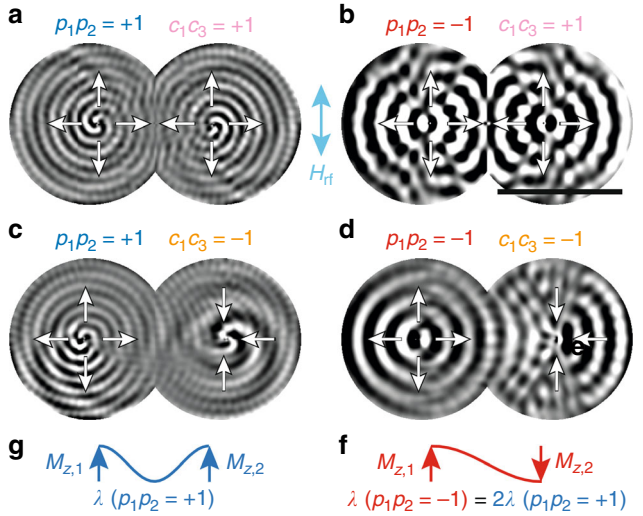

Fig. 4 Micromagnetic simulations of spin-wave interferences. **a**–**d** Snapshots of the z-component of the magnetisation M_z of the corresponding stable states shown in Fig. 2. For better visibility the static contrast is subtracted and the contrast is oversaturated. The excitation frequency and field amplitude are $f_{rf} = 6$ GHz and $\mu_0 H_{rf} = 0.5$ mT. The white arrows indicate the propagation direction of the short-wavelength spin-wave modes. **a** Antivortex state with equal polarisations in the stacks. **b** Antivortex state with different polarisations. **c** Diamond state with equal polarisations and **d** with opposing polarisations in the stacks. **e**, **f** Representation of the magnetisation of the vortex cores in one stack for equal (**e**) and opposite (**f**) polarisations and assigned wavelengths of the spin waves. Scale bar: 1 μm

antivortices in the centre do not seem to emit spin waves themselves. The amplitude of the spin wave varies over time and space. This behaviour is observed most pronouncedly in the antivortex state with opposite polarisations of the vortices on top of each other (Fig. 4b). Here, concentric, outwards-travelling spin waves are emitted by the two vortex stacks. The spin waves have a wavelength of 170 nm, thus approximately twice the wavelength of the spin waves in Fig. 4a. The interference of the spin waves leads to a variation of the spin-wave amplitude and an increase of the overall spin-wave amplitude along the x-direction compared to the y-direction. Thus, in the case of Fig. 4b the spin-wave amplitude is confined in the x-direction (see also Supplementary Movie 3b).

Snapshots of the dynamics of the diamond magnetisation state are depicted in Fig. 4c, d. In the case of equal polarisations (Fig. 4c), spiral-shaped spin waves with a wavelength of 90 nm are emitted by the left stack. In the right stack, a short-wavelength mode travels inwards as indicated by the white arrows. Since an outwards propagating long-wavelength mode is superimposed, the identification of the inwards propagating short spin waves requires a close observation of the data in Supplementary Movie 3c. Figure 4d shows the steady state motion of a diamond magnetisation state with opposite polarisations in a stack ($p_1p_2 = -1$). As in the antivortex state, the vortices emit concentric spin waves with twice the wavelength compared to the state with equal polarisations. In the left stack a nearly undisturbed outwards propagating spin wave is observed. In the right stack, the spin waves propagate inwards and interfere with the spin waves emitted by the left stack. The dynamics show a pronounced interference pattern, as well as an increase of the overall spin-wave amplitude along the x-direction compared to the y-direction.

Despite the complexity of the stacked vortex system, simple rules for the general behaviour of the spin waves apply. Most obvious is the wavelength of the spin waves when considering Fig. 4a–d. A short-wavelength spin wave (90 nm) is generated whenever $p_1p_2 = +1$ and a longer wavelength spin wave (170 nm) is generated if $p_1p_2 = -1$. A vivid explanation for the emergence of spin waves with different wavelengths can be derived from the source of the spin waves. Two gyrating stacked vortex cores lead to local perturbations of the z-component of the magnetisation M_z that give rise to the outwards travelling spin waves[10]. Neglecting that the two vortex cores are not in the same layer we assign possible wavelengths for such perturbations of the z-component of the magnetisation M_z in Fig. 4e, f. In the $p_1p_2 = +1$ case (blue), a first order wave that has half the wavelength compared to the $p_1p_2 = -1$ case (red) can be assigned and explains the observed spin-wave wavelengths. The second prominent feature when examining Fig. 4a–d is the appearance of spiral-shaped spin waves for $p_1p_2 = +1$ and concentric spin waves for $p_1p_2 = -1$. A possible explanation can be derived from the gyration direction of the vortex cores that depends on the polarisation. The spin-wave source has a non-vanishing total angular momentum in the $p_1p_2 = +1$ case as the cores gyrate in the same direction, whereas in the $p_1p_2 = -1$ case the cores gyrate in opposite directions and the total angular momentum vanishes. Thus, in the $p_1p_2 = -1$ case the two motions quench the total angular momentum leading to concentric spin waves while they add up in the case of parallel aligned cores ($p_1p_2 = +1$), leading to spiral spin waves (compare also Supplementary Fig. 3). These two vivid explanations only account for the generation process of the spin waves and do not consider reflection or interference of spin waves.

The micromagnetic simulations lead us to suggest that it is possible to observe spin-wave interferences in two exchange-coupled stacks of magnetic vortices. The diamond magnetisation state with different polarisations in the stacks (Fig. 4d) shows the most pronounced interference. Our system provides an excellent controllability of spin-wave properties. Tuning of the circularity configurations[22,23] can be used to manipulate the propagation direction of the spin waves as most prominently seen in Fig. 4b, d as well as in the corresponding Supplementary Movie 3b, d. Tuning of the polarisation configuration[24–27] can be used to manipulate the wavelength and shape of the spin waves. The interference offers the possibility to confine the information at distinct points in space. This is crucial for the use of spin waves in future magnonic devices.

Experimental observation of spin-wave interferences. We now compare the micromagnetic simulations to the experimental findings. In Fig. 5a, b snapshots of two exemplary STXM measurements are shown, in Fig. 5c, d the corresponding micromagnetic simulations are depicted (see also Supplementary Movie 4 for the corresponding movies). The stable magnetisation configurations corresponding to the dynamics are illustrated in Fig. 5e, f. In Fig. 5a the vortices are excited with a high-frequency magnetic field with a frequency of $f_{rf} = 4.978$ GHz and an amplitude of $\mu_0 H_{rf} = 0.2$ mT[28]. The vortices in the left stack emit concentric, outwards-propagating spin waves with a wavelength of 215 nm. The vortices on the right side emit spin waves that propagate inwards with the same wavelength. These spin waves interfere with each other as can be seen from the typical interference pattern, i.e., a cone-like region with high-amplitude spin waves in the right stack that is surrounded by a low-amplitude region. This interference pattern strongly resembles the micromagnetic simulation of a diamond magnetisation state with opposite polarisations in a stack that is shown for comparison in Fig. 5c, e. The propagation direction of the spin waves depends on the absolute orientation of the circularities in the stacks (c_1, c_2)

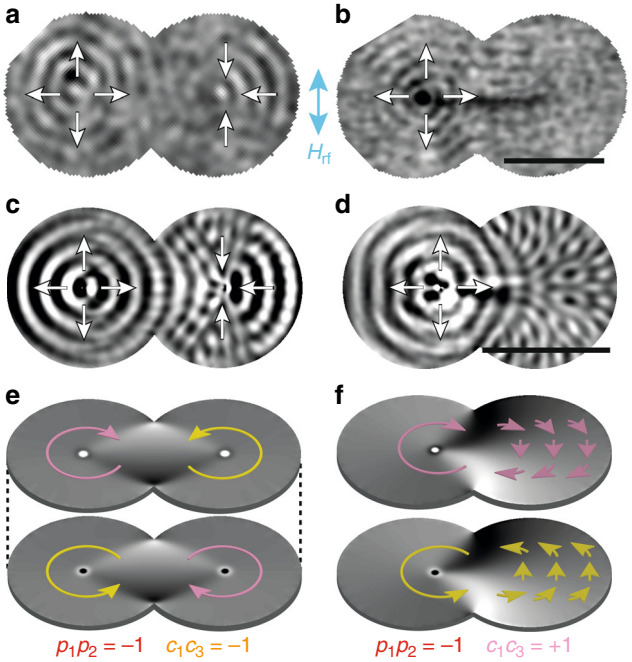

Fig. 5 Comparison of experiments and micromagnetic simulations. **a**, **b** Normalised STXM data of two magnetisation configurations. The white arrows show the propagation direction of the spin waves. In (**a**) the black and white contrast shows the z-component of the magnetisation M_z for an excitation $f_{rf} = 4.978$ GHz and $\mu_0 H_{rf} = 0.2$ mT. In (**b**) the sample is tilted by 30° with respect to the beam axis. The excitation frequency and field amplitude are $f_{rf} = 5.891$ GHz and $\mu_0 H_{rf} = 0.33$ mT. **c**, **d** Normalised micromagnetic simulations of the spin-wave emission in two different stable magnetisation configurations corresponding to (**a**, **b**). (**c**) shows the M_z component and (**d**) the sum of $M_{x,y,z}$ to account for the tilt of the sample in the experiments. The excitation frequency and field amplitude are $f_{rf} = 6$ GHz and $\mu_0 H_{rf} = 0.5$ mT. **e**, **f** Micromagnetic simulations of the stable magnetisation configurations corresponding to the dynamics shown in (**c**, **d**). The yellow and pink arrows represent the in-plane magnetisation, i.e. a circularity of $c = +1$ and $c = -1$, respectively. Scale bars: 1 µm

and (c_3, c_4). We make sure that the circularities in the experiments and simulations are equally oriented. The concentric form of the spin waves and their wavelength lead to the conclusion that the polarisations in the stacks are aligned antiparallel in the experiments ($p_1p_2 = -1$ and $p_3p_4 = -1$). The wavelength of the spin waves is in qualitative and quantitative agreement with the simulations for $p_1p_2 = -1$ as can be seen in Supplementary Note 2, Supplementary Fig. 2, where the dispersion relations of theoretically predicted spin-wave modes are compared to the micromagnetic simulations and experiments. Thus, we directly observe spin-wave interference in exchange-coupled stacks of vortices. Due to the interference, the amplitude of the spin waves varies in the structure with distinct areas of low and high spin-wave amplitudes. In addition to spin-wave interference, spin-wave diffraction is observed in another structure (Fig. 5b). The vortices are excited with a high-frequency magnetic field with a frequency of $f_{rf} = 5.891$ GHz and an amplitude of $\mu_0 H_{rf} = 0.33$ mT. Here, vortices are only present in the left stack. They emit spin waves that propagate outwards and have a wavelength of 176 nm. The spin waves travel to the right stack that does not contain any vortices where the amplitude of the spin waves is reduced. This spin wave pattern is also reproduced by the micromagnetic simulations: Fig. 5d shows a snapshot of a micromagnetic simulation of the spin-wave dynamics of the stable state depicted in Fig. 5f (see also Supplementary Movie 4d).

The stable magnetisation configuration with vortices in only one stack is found in exchange-coupled permalloy stacks with an increased percentile overlap (25% compared to 18.5%, Fig. 5f). The propagation direction of the spin waves, their concentric form, and their wavelength lead to the conclusion that the magnetisation state in the experiments and simulations coincides. The vortices in the left stack emit spin waves that travel to the right stack (Fig. 5b, d). The spin waves are diffracted at the constriction and a diffraction pattern is visible at the right side of the structure. Due to diffraction, the amplitude of the emitted spin waves decreases in the right side of the structure. The experimentally observed spin-wave dynamics are in excellent agreement with the micromagnetic simulations.

Discussion

We have shown experimentally that spin-wave interference and diffraction can be directly observed and controlled in exchange-coupled stacks of magnetic vortices. These stacks generate spin waves with a wavelength in the 100 nm regime. The experiments are precisely reproduced by micromagnetic simulations and are understood in a simplified vivid explanation. The amplitude of the spin waves varies in the structure thus creating distinct areas of low and high spin-wave amplitudes. This is an important feature for the use of vortices as spin-wave emitters in, e.g. spin-wave-based signal-processing devices. A cascade of the investigated structure might be used as an efficient way to carry and process information in such a device.

Methods

Sample preparation. Vortex stacks consisting of two permalloy ($Ni_{80}Fe_{20}$) and two silicon layers are prepared by electron-beam lithography, O_2 plasma etching, thermal evaporation, and lift-off processing on 100-nm-thick silicon-nitride membranes transparent for soft X-rays. The permalloy layers have a height of $t_{Py} = 50$ nm and are separated and covered by silicon layers of $t_{Si} = 10$ nm in height. The radius of the disks is $r = 800$ nm and the overlap is $o = 300$ nm. An ensemble of 180 structures is deposited on a coplanar waveguide with a thickness of 100 nm of copper and a hydrogen silsesquioxane (HSQ) isolation layer of 40 nm.

STXM measurements. The spin-wave dynamics are directly observed using STXM at the MAXYMUS microscope of the BESSY II synchrotron in Berlin, Germany. The magnetic contrast is provided via the X-ray magnetic circular dichroism at the Ni L_3 absorption edge ($E \approx 854$ eV). In the mode of operation used here, the setup provides a spatial resolution of 25 nm and a temporal resolution of 100 ps. The magnetisation dynamics are stroboscopically imaged. If the sample is placed perpendicular to the beam axis, the z-component of the magnetisation M_z is measured. If the sample is tilted by 30° with respect to the beam axis, additionally one in-plane component of the magnetisation is visible. Using the tilted setup, the circularity configurations in the stacks are determined to $c_1c_2 = -1$ and $c_3c_4 = -1$.

Micromagnetic simulations. The micromagnetic simulations are performed using the MicroMagnum micromagnetic simulation software[20]. In the simulations, the structures are slightly smaller than in the experiments in order to comply with memory constraints of the graphics processing units. The disk's radius and overlap are $r = 640$ nm and $o = 240$ nm. The height of the two permalloy layers is $t_{Py} = 40$ nm. In the simulations the 10 nm spacing between the layers is modelled using vacuum. The sample size was chosen so that the disks have the same aspect ratio $\frac{t_{Py}}{r}$ as the disks in the experiment ensuring an identical resonance frequency with respect to the experiment[15]. The interlayer thickness is held constant as this parameter is expected to influence the dispersion relation of the spin-wave modes dominantly. Given the chosen parameters, the gradient of the expected dispersion relation is increased by only 1.2% compared to the dispersion relation with the parameters of the experiments[10]. The cell size is $4 \times 4 \times 5$ nm^3. Standard permalloy material parameters are used: a saturation magnetisation $M_s = 800$ kA m^{-1}, an exchange stiffness constant of $A_{ex} = 1.3 \times 10^{-11}$ Jm^{-1}, and a Gilbert damping constant of $\alpha = 0.01$. A linear alternating magnetic field is applied in y-direction with an amplitude of $\mu_0 H_{rf} = 0.5$ mT and a frequency of $f_{rf} = 6$ GHz.
We performed a limited number of simulations using a different cell size of $5 \times 5 \times 5$ nm^3 with the sample dimensions used in the experiments (not shown in the manuscript). These simulations qualitatively show the same behaviour as the simulations of the smaller structures.

Data availability

The data that support the findings of this study are available from the corresponding author upon reasonable request.

Received: 11 April 2018 Accepted: 8 August 2018
Published online: 04 September 2018

References

1. Demidov, V. E., Urazhdin, S. & Demokritov, S. O. Direct observation and mapping of spin waves emitted by spin-torque nano-oscillators. *Nat. Mater.* **9**, 984–988 (2010).
2. Wang, Q. et al. Reconfigurable nanoscale spin-wave directional coupler. *Sci. Adv.* **4**, e1701517 (2018).
3. Chumak, A. V., Serga, A. A. & Hillebrands, B. Magnonic crystals for data processing. *J. Phys. D. Appl. Phys.* **50**, 244001 (2017).
4. Jamali, M., Kwon, J. H., Seo, S.-M., Lee, K.-J. & Yang, H. Spin wave nonreciprocity for logic device applications. *Sci. Rep.* **3**, 3160 (2013).
5. Woo, S., Delaney, T. & Beach, G. S. D. Magnetic domain wall depinning assisted by spin wave bursts. *Nat. Phys.* **13**, 448–454 (2017).
6. Choi, S., Lee, K.-S. & Kim, S.-K. Spin-wave interference. *Appl. Phys. Lett.* **89**, 062501 (2006).
7. Macià, F., Kent, A. D. & Hoppensteadt, F. C. Spin-wave interference patterns created by spin-torque nano-oscillators for memory and computation. *Nanotechnology* **22**, 095301 (2011).
8. Mukherjee, S. S., Kwon, J. H., Jamali, M., Hayashi, M. & Yang, H. Interference-mediated modulation of spin waves. *Phys. Rev. B* **85**, 224408 (2012).
9. Vogt, K. et al. Realization of a spin-wave multiplexer. *Nat. Commun.* **5**, 3727 (2014).
10. Wintz, S. et al. Magnetic vortex cores as tunable spin-wave emitters. *Nat. Nanotechnol.* **11**, 948–953 (2016).
11. Shinjo, T., Okuno, T., Hassdorf, R., Shigeto, K. & Ono, T. Magnetic vortex core observation in circular dots of permalloy. *Science* **289**, 930–932 (2000).
12. Wachowiak, A. et al. Direct observation of internal spin structure of magnetic vortex cores. *Science* **298**, 577–580 (2002).
13. Van Waeyenberge, B. et al. Magnetic vortex core reversal by excitation with short bursts of an alternating field. *Nature* **444**, 461–464 (2006).
14. Kamionka, T. et al. Magnetic antivortex-core reversal by circular-rotational spin currents. *Phys. Rev. Lett.* **105**, 137204 (2010).
15. Guslienko, K. Y. et al. Eigenfrequencies of vortex state excitations in magnetic submicron-size disks. *J. Appl. Phys.* **91**, 8037–8039 (2002).
16. Choe, S.-B. et al. Vortex core–driven magnetisation dynamics. *Science* **304**, 420–422 (2004).
17. Kammerer, M. et al. Magnetic vortex core reversal by excitation of spin waves. *Nat. Commun.* **2**, 279 (2011).
18. Choi, S., Lee, K.-S., Guslienko, K. Y. & Kim, S.-K. Strong radiation of spin waves by core reversal of a magnetic vortex and their wave behaviors in magnetic nanowire waveguides. *Phys. Rev. Lett.* **98**, 087205 (2007).
19. Park, J. P. & Crowell, P. A. Interactions of spin waves with a magnetic vortex. *Phys. Rev. Lett.* **95**, 167201 (2005).
20. Micromagnum. http://micromagnum.informatik.uni-hamburg.de/ (2013).
21. Shigeto, K., Okuno, T., Mibu, K., Shinjo, T. & Ono, T. Magnetic force microscopy observation of antivortex core with perpendicular magnetization in patterned thin film of permalloy. *Appl. Phys. Lett.* **80**, 4190–4192 (2002).
22. Im, M.-Y. et al. Stochastic formation of magnetic vortex structures in asymmetric disks triggered by chaotic dynamics. *Nat. Commun.* **5**, 5620 (2014).
23. Velten, S. et al. Vortex circulation patterns in planar microdisk arrays. *Appl. Phys. Lett.* **110**, 262406 (2017).
24. Hänze, M., Adolff, C. F., Velten, S., Weigand, M. & Meier, G. Two-body problem of core-region coupled magnetic vortex stacks. *Phys. Rev. B* **93**, 054411 (2016).
25. Adolff, C. F. et al. Self-organized state formation in magnonic vortex crystals. *Phys. Rev. B* **88**, 224425 (2013).
26. Hänze, M., Adolff, C. F., Weigand, M. & Meier, G. Burst-mode manipulation of magnonic vortex crystals. *Phys. Rev. B* **91**, 104428 (2015).
27. Jain, S. et al. From chaos to selective ordering of vortex cores in interacting mesomagnets. *Nat. Commun.* **3**, 1330 (2012).
28. Silva, T. J., Lee, C. S., Crawford, T. M. & Rogers, C. T. Inductive measurement of ultrafast magnetization dynamics in thin-film Permalloy. *J. Appl. Phys.* **85**, 7849–7862 (1999).

Acknowledgements

We thank Ulrich Merkt for fruitful discussions and Michael Volkmann for superb technical assistance. We acknowledge the support of the Max-Planck-Institute for Intelligent Systems (formerly MPI for Metals Research), Department Schütz and the MAXYMUS team, particularly Michael Bechtel and Eberhard Goering. We thank the Helmholtz-Zentrum Berlin für Materialien und Energie for the allocation of synchrotron radiation beamtime. Financial support of the Deutsche Forschungsgemeinschaft via the Sonderforschungsbereich 668 is gratefully acknowledged. This work has been supported by the excellence cluster 'The Hamburg Centre for Ultrafast Imaging - Structure, Dynamics, and the Centre of Matter at the Atomic Scale' of the Deutsche Forschungsgemeinschaft.

Author contributions

C.B., C.F.A., M.H., B.S., and G.M. designed the study. C.B., N.L., and M.W. conducted the measurements at the MAXYMUS microscope with support from G.S. C.B. prepared the samples. C.B. and N.L. performed the micromagnetic simulations. C.B., C.F.A., and G.M. wrote the manuscript. All authors commented on the final manuscript.

Additional information

Supplementary Information accompanies this paper at https://doi.org/10.1038/s42005-018-0052-1.

Competing interests: The authors declare no competing interests.

Reprints and permission information is available online at http://npg.nature.com/reprintsandpermissions/

Publisher's note: Springer Nature remains neutral with regard to jurisdictional claims in published maps and institutional affiliations.

Open Access This article is licensed under a Creative Commons Attribution 4.0 International License, which permits use, sharing, adaptation, distribution and reproduction in any medium or format, as long as you give appropriate credit to the original author(s) and the source, provide a link to the Creative Commons license, and indicate if changes were made. The images or other third party material in this article are included in the article's Creative Commons license, unless indicated otherwise in a credit line to the material. If material is not included in the article's Creative Commons license and your intended use is not permitted by statutory regulation or exceeds the permitted use, you will need to obtain permission directly from the copyright holder. To view a copy of this license, visit http://creativecommons.org/licenses/by/4.0/.

© The Author(s) 2018